Optical Engineering

OpticalEngineering.SPIEDigitalLibrary.org

Planar concave grating wavelength demultiplexers with flattened spectral response based on SU-8 polymer waveguides

Guomin Jiang
Sarfaraz Baig
Hui Lu
Kai Shen
Michael R. Wang

SPIE.

Guomin Jiang, Sarfaraz Baig, Hui Lu, Kai Shen, Michael R. Wang, "Planar concave grating wavelength demultiplexers with flattened spectral response based on SU-8 polymer waveguides," *Opt. Eng.* **55**(3), 037104 (2016), doi: 10.1117/1.OE.55.3.037104.

Planar concave grating wavelength demultiplexers with flattened spectral response based on SU-8 polymer waveguides

Guomin Jiang,[a] Sarfaraz Baig,[b] Hui Lu,[a] Kai Shen,[a] and Michael R. Wang[a,*]
[a]University of Miami, Department of Electrical and Computer Engineering, 1251 Memorial Drive, Coral Gables, Florida 33146, United States
[b]University of Miami, Department of Biomedical Engineering, 1251 Memorial Drive, Coral Gables, Florida 33146, United States

Abstract. Planar concave grating wavelength demultiplexers with a flattened spectral response are realized based on SU-8 polymer waveguides. The flattened spectral response is accomplished by using an optimized multimode interference (MMI) coupler as the input aperture of the planar waveguide for all spectrally separated channels. The mode field distribution at the input of the planar waveguide is controlled by adjusting the width of the input taper connected to the MMI coupler. The devices are fabricated by cost-effective one-step UV lithography. Experimental results show that the desired flattened spectral response has been realized. The on-chip loss, crosstalk, and nonuniformity of the fabricated device are −14.8, −22, and 2.5 dB, respectively. © *2016 Society of Photo-Optical Instrumentation Engineers (SPIE)* [DOI: 10.1117/1.OE.55.3.037104]

Keywords: wavelength division multiplexing; gratings; multimode interference coupler; polymer waveguides; SU-8.

Paper 151660P received Nov. 24, 2015; accepted for publication Feb. 19, 2016; published online Mar. 11, 2016.

1 Introduction

The demand for high aggregate capacity and bandwidth for optical interconnection and communication requires the development of wavelength division multiplexing (WDM) systems. Many different waveguide WDM techniques have been proposed, mainly including planar concave grating (PCG), arrayed waveguide grating (AWG), ring resonators, and Mach–Zehnder interferometers.[1–5] PCG and AWG have been widely researched and have made great progress due to their low cost, large fabrication tolerance, and high performance. We consider the PCG structure because of its significant size advantage over AWG.[5–7] A typical PCG structure has a Gaussian-like spectral response with high sensitivity to small spectral shifts, which seriously restricts its practical application in dense or coarse WDM systems.[7] A flat spectral response is desirable for large spectral shift tolerance that can be realized by using a multimode interference (MMI) coupler section in connection to the PCG planar waveguide.[8–10]

There are various optical waveguides with different materials for realizing PCG devices, including silica, semiconductors, and polymers. In silica-on-silicon[3] and InP,[11] a large bending radius is generally required due to low refractive index (RI) contrast waveguide, which results in relatively large device size and low-density on-chip integration. In silicon-on-insulator,[5] one can realize ultracompact PCG because of the high RI contrast waveguides and associated sharp waveguide bending. However, expensive lithography techniques such as deep UV or E-beam lithography are usually required for silicon photonic device fabrication due to the submicron cross-section dimension.[12,13] The silicon waveguide is not suitable for the application in visible to near infrared below the 1100-nm wavelength.

Polymer has the obvious advantages of a wide spectral transparent window, high flexibility, and low-cost fabrication.[14,15] SU-8 polymer in particular is an attractive photosensitive polymeric material for the fabrication of planar lightwave circuits because of its easy fabrication and relatively good chemical and thermal stabilities.[16–20] To support cost-effective integration with polymer-based optical interconnection and to facilitate minimal interface loss with fiber-based optical communication networks, we consider SU-8 polymer for the implementation of the PCG wavelength demultiplexer in this paper. For large RI contrast, we use polymer waveguide with an air cladding.[17,20]

In this paper, we present four-channel PCG wavelength demultiplexers on SU-8 polymer waveguides with a flattened spectral response. The flattened spectral response is accomplished by using an optimized MMI as the PCG planar waveguide input for all spectrally separated channels. The mode field distribution at the PCG planar waveguide input is controlled by adjusting the waveguide taper width coupled to the MMI instead of the MMI width or length.[9] The devices are realized by using SU-8 polymer waveguides fabricated by a one-step UV lithography process, offering lower cost and wider spectral band selection flexibility. The PCG wavelength demultiplexer with the desired flattened spectral response has been demonstrated.

2 Theory

Figure 1 shows the schematic diagram of the MMI-PCG based on conventional Rowland circle geometry.[21] The input and output waveguides are positioned along the Rowland circle with a radius R. The grating facets are located on a grating circle with a radius equal to the diameter of the Rowland circle. The grating circle and Rowland circle touch at the center of the grating. There is a planar waveguide region between the input/output channel waveguides and the concave grating. The input light diverges toward the

*Address all correspondence to: Michael R. Wang, E-mail: mwang@miami.edu

0091-3286/2016/$25.00 © 2016 SPIE

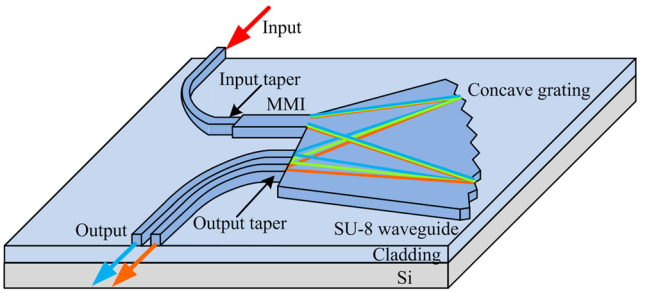

Fig. 1 Schematic diagram of MMI-PCG.

grating in this planar free propagation region. The concave grating on the grating circle diffracts back and focuses the light into the output waveguides on the Rowland circle. The positions of the input and output waveguides are determined by the grating equation[5]

$$d(\sin\theta_i + \sin\theta_d) = m\lambda/n_{\text{eff}}, \tag{1}$$

where θ_i and θ_d are the incident and diffracted angles with respect to the grating circle normal at the center of the grating. d is the period of the grating, m is the diffraction order, λ is the wavelength in free space, and n_{eff} is the effective index of the planar waveguide mode at wavelength λ.

The MMI aperture located on the input port of the PCG planar waveguide is used as a mode shaper to form a flat field distribution. It consists of a taper with width w and a multimode section with length L and width W, as shown in Fig. 2. The input taper of the MMI is located at the center of the MMI for a symmetric interference. According to the self-imaging principle of MMI, an input field profile is reproduced in single or multiple images along the propagation direction of the MMI waveguide.[22] The location z of the first N images of the input field distribution can be calculated from

$$z = 3\pi/4N(\beta_0 - \beta_1), \tag{2}$$

where β_0 and β_1 are the propagation constants of the first two lowest modes of the MMI. Any N images location can be

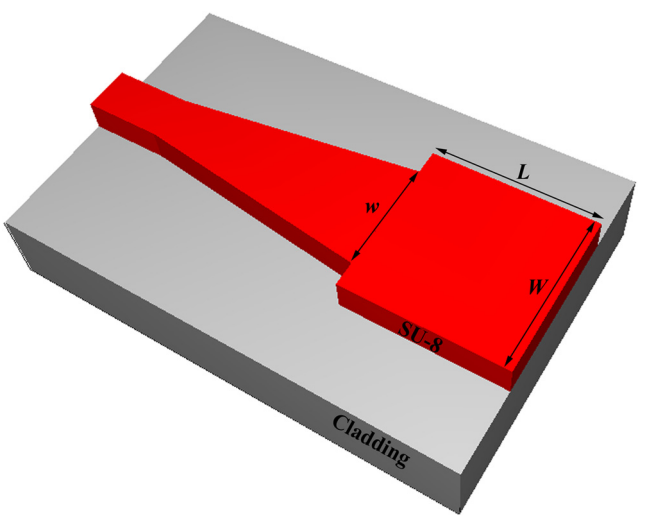

Fig. 2 Schematic of an MMI aperture for a PCG planar waveguide.

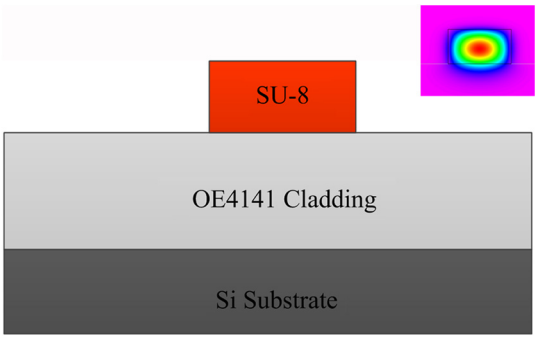

Fig. 3 Cross-section of an SU-8 strip waveguide. The insert shows the calculated fundamental mode profile for the 2.5 μm wide and 2 μm high waveguide.

chosen for the flat field output of the MMI aperture. The width W of the MMI can be utilized for changing the distance between the center positions of N images. The width w of the input taper can be used for defining the field distribution of each image and changing their overlap. The parameters w, W, and L of the MMI aperture can be adjusted to control the mode field distribution at the input of the PCG planar waveguide. The convolution of this imaged flat field on the Rowland circle and the output aperture mode of the PCG planar waveguide will produce a flattened spectral response.[9] The width of the flat region in the spectral response depends on the width of the field distribution of the MMI aperture.

Figure 3 shows the cross-section of a small SU-8 (Microchem) ridge waveguide with an air top cladding and OE4141 (Dow Corning) photopolymer bottom cladding on a Si substrate. The refractive indices of SU-8 and OE4141 are 1.575 and 1.494, respectively, at the 1310 nm wavelength. The optical channel waveguides for the device input and output have 2.5-μm width and 2-μm height, satisfying the single-mode condition calculated by the finite-difference method. All waveguide structures are designed for transverse electric (TE) polarization in this paper. The inset in the right corner of Fig. 3 shows the calculated fundamental (TE_{00}) mode profile. All the PCG input and output channel waveguides have a bend radius of 300 μm. The output channel waveguide has a 300 μm long waveguide taper that changes width from a 5-μm aperture to 2.5 μm wide waveguide. The width w of the 300 μm long input taper of MMI has been optimized as discussed below.

3 Design of Multimode Interference and Planar Concave Grating

The length L of the MMI aperture is chosen at two image locations for flat field output in this paper because of its better flat top performance and larger tolerance compared with other N image locations. The flat field width of the MMI aperture should be comparable to the width of the PCG output aperture to create a sufficiently flat image. A 10 μm wide W MMI aperture with about a 5 μm wide flat top profile (close to the width of the PCG output aperture) are the best compromise for achieving a low loss and flat spectral response. The decrement in width W will produce a lower loss but have a narrower spectral response. The increment in width W will have a wider spectral response but significantly increase the loss. The required length L of a 10 μm

wide MMI aperture for the two image positions is calculated to be 60.8 μm from Eq. (2).

The simulated field distribution for the 10 μm wide and up to 122 μm long MMI couplers with input taper widths w of 4.0, 6.0, 7.0, 7.7, and 9.0 μm are shown in Fig. 4. Two images of the input field profile are clearly reproduced at the $L = 60.8$ μm position (dotted line). A line scan of the field distribution at the two image positions of these MMI apertures is shown in Fig. 5. The field distribution of these two images in combination changes from a twofold image with a center dip to a Gaussian-like curve by varying the input taper width w from 4.0 to 9.0 μm. The spectral response of the device can be obtained from the convolution of the waveguide mode field profile of the PCG output aperture (black solid line) with the imaged field distributions of the MMI aperture on the output plane.

The PCG is designed around a central wavelength λ of 1310 nm. The diffraction order m is chosen to be 10 in this study, which results in a free spectral range of about 130 nm. The total internal reflection facet is applied to the PCG grating. The incident and diffracted angles are chosen to be 65 deg and −25 deg, respectively. The calculated grating period d is 17.4 μm from Eq. (1). The 5 μm wide tapered output waveguides are spaced 10 μm apart on the Rowland circle. The designed central wavelengths of the four output channels are 1280, 1300, 1320, and 1340 nm, with 20 nm spectral separations. The Rowland circle radius R is then 613.6 μm.

The PCG simulation is performed based on the scalar diffraction theory.[5] The field distribution at the end of the MMI is calculated by BeamPROP (Rsoft), which is used as the input field of the PCG planar waveguide. The incident waveguide field on the grating facets and the diffracted field on the Rowland circle are calculated according to the Kirchhoff–Huygens diffraction formula. The spectral response of each channel can be obtained by calculating the overlap integral

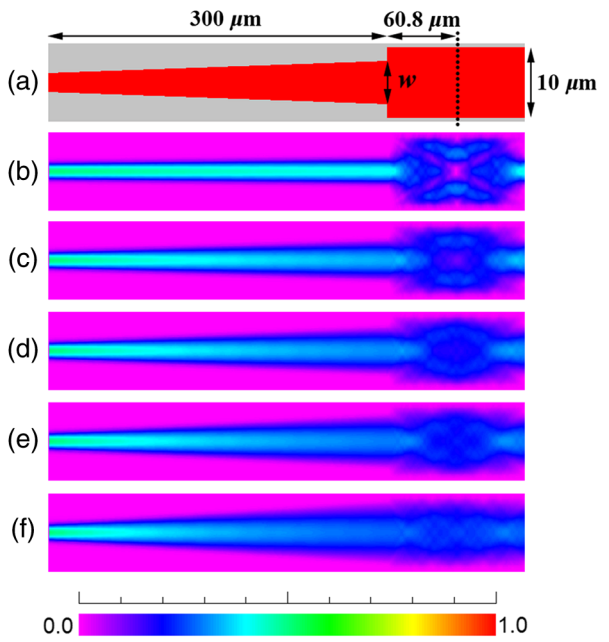

Fig. 4 (a) Schematic geometry of MMI aperture. (b)–(f) Simulated field distribution of 10 μm wide MMIs with input taper widths w of 4.0 μm, 6.0 μm, 7.0 μm, 7.7 μm, and 9.0 μm, respectively.

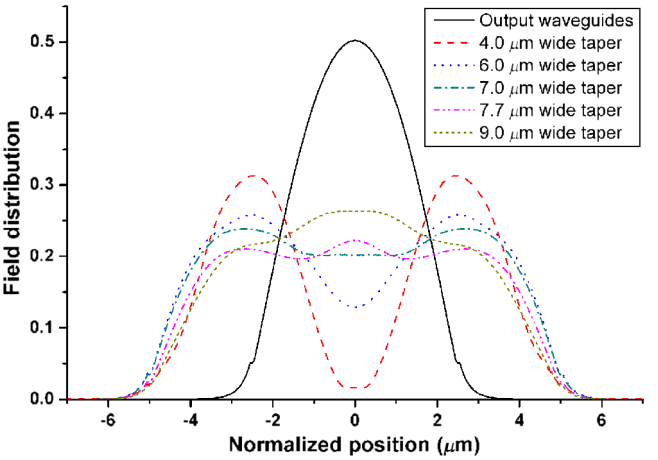

Fig. 5 Mode field distribution at the two image positions of MMI apertures for different input taper widths w.

between the mode field profile of the PCG output aperture and the diffracted and focused field of the PCG on the Rowland circle. The grating facets are chipped and blazed[23] for better performance (higher peak transmission and lower crosstalk). The grating reflection is set to 100% for these simulations. The simulated spectral response of the MMI-PCGs shows the change from a center dip shape to a Gaussian-like shape by varying the width of the input taper from 4.0 to 9.0 μm. Figure 6(a) shows the simulated spectral response of the MMI-PCGs with four different input taper widths (4.0, 6.0, 7.7, and 9.0 μm). We get a flat spectral response at 7.7 μm of the input taper width. If the taper width is 4.0 or 6.0 μm smaller than the optimized taper width 7.7 μm, the device indicates a center dip spectral response. If the taper width is 9.0 μm wider than 7.7 μm, the device approaches a Gaussian-like spectral response. The simulated transmission spectrum of the MMI-PCG with 7.7 μm wide input taper is shown in Fig. 6(b). The device exhibits a central channel loss of −6.2 dB, a crosstalk of −36.6 dB, and an on-chip loss nonuniformity of 0.3 dB.

4 Fabrication

To verify the device design, MMI-PCG devices with different input taper widths w were fabricated on SU-8 polymer. Only a one-step UV lithography process is needed, which greatly simplifies the fabrication process.[17,19] We first spin-coated an 8 μm thick OE4141 cladding layer on top of a cleaned Si substrate and cured it by flood UV exposure. It has a very good optical property and is thick enough to avoid waveguide mode leakage to the Si substrate. A 2 μm thick SU-8 polymer film was then formed on the cladding layer by a spin-coating process. The Si wafer with an SU-8 core layer was prebaked with two steps (1 min @ 65°C and 1 min @ 95°C) on a hotplate to evaporate the solvent. Then, the patterns on the photomask were transformed to the SU-8 film by i-line UV photolithography. The Si wafer with the exposed SU-8 film was then postbaked (1 min @ 65°C and 2 min @ 95°C) to finish the polymer cross-linking process. Following development and rinsing, the final MMI-PCG device with the SU-8 planar and channel waveguides was obtained. A short hard baking time (1 min @ 65°C and 5 min @ 150°C) is preferred to smooth the waveguide

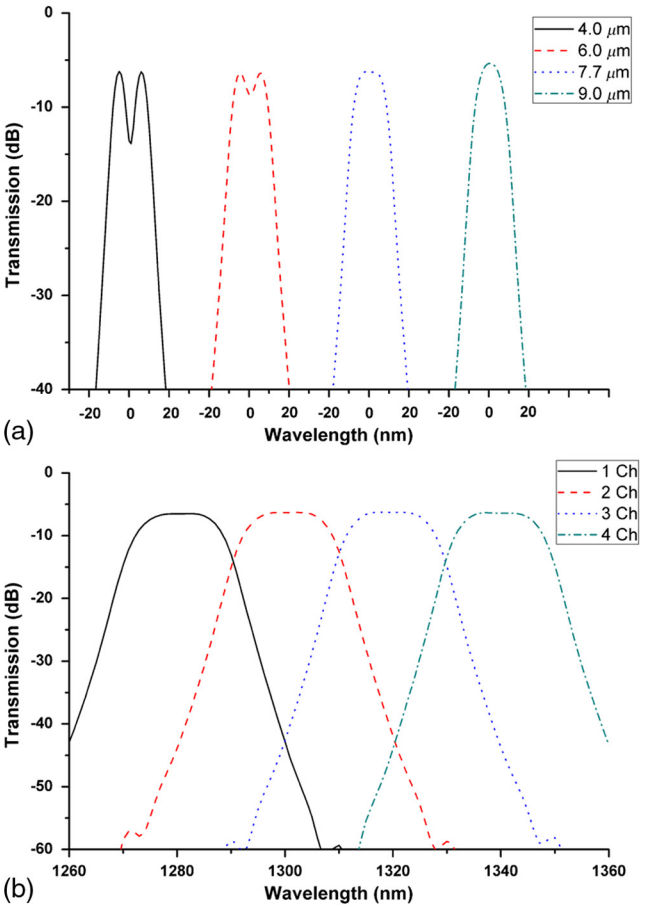

Fig. 6 Simulation spectral response of (a) MMI-PCGs with variation of input taper width w and (b) MMI-PCG with 7.7 μm wide input taper.

sidewalls and reduce the scattering loss while keeping the sidewall vertical.[17]

Figure 7 shows the microscope images of the fabricated MMI-PCG device. A series of strip waveguides was also fabricated on the same chip for reference. Figure 8 shows the cross-section view of the fabricated SU-8 strip optical waveguide with 2.5 μm width and 1.7 μm height, which is slightly thinner than our design. The 1310-nm input light from the light source fiber was butt-coupled to the input

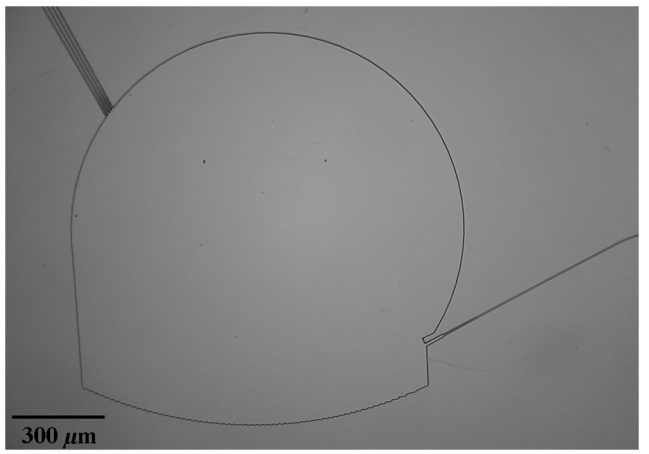

Fig. 7 Microscope images of the fabricated MMI-PCG device.

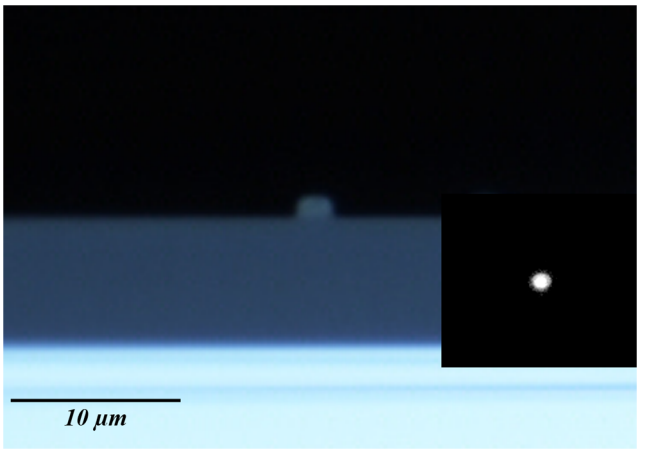

Fig. 8 Microscope images of the cross-section view of the SU-8 optical waveguide. The insert shows the mode profile of the fabricated waveguide.

waveguide through a tapered lens fiber with a focus spot size of about 2.5 μm. A 60× microscope objective lens was used to collect the output light from the end of the output optical waveguides, and was connected to an infrared camera (Electrophysics Microviewer 7290). The insert picture shows the mode profile of the waveguide, indicating a single mode propagation in the fabricated SU-8 optical waveguide. The propagation loss of a straight SU-8 waveguide was about −0.6 dB/mm measured by the conventional cut back method at the 1310 nm wavelength.

5 Measurement and Discussion

A broadband superluminescent diode light source was used to characterize the fabricated MMI-PCG devices. A tapered lens fiber was used to butt-couple the input light from the light source to the input channel waveguide. Another tapered lens fiber was used to collect the output light from the end of output channel waveguides, and was connected to an optical spectrum analyzer (Agilent 86142B). The input fiber was aligned and fixed to the input channel waveguide of an MMI-PCG by maximizing the output power to the second output channel waveguide (counted from the long wavelength). Then, we aligned the output fiber to each output channel waveguide and recorded its spectral response. The same procedure was used for the measurement of all other devices.

The measured spectral response of the fabricated MMI-PCG devices with four different input taper widths (4.0, 6.0, 7.0, and 8.0 μm) is shown in Fig. 9(a). The losses are normalized to a reference straight waveguide. The MMI-PCG devices with 4.0 and 6.0 μm wide input tapers show the center dip spectral response, while the one with the 8.0 μm wide input taper shows a near Gaussian-shaped spectral response. The device with the 7.0 μm wide input taper presents the most flattened spectral response, which is slightly different from simulation results, due most likely to the small mismatch between the fabricated MMI width and waveguide height and the values used in the design simulation.

Figure 9(b) shows the measured transmission spectrum of the fabricated MMI-PCG device with the 7.0 μm wide input taper. The on-chip loss for the central wavelength is about

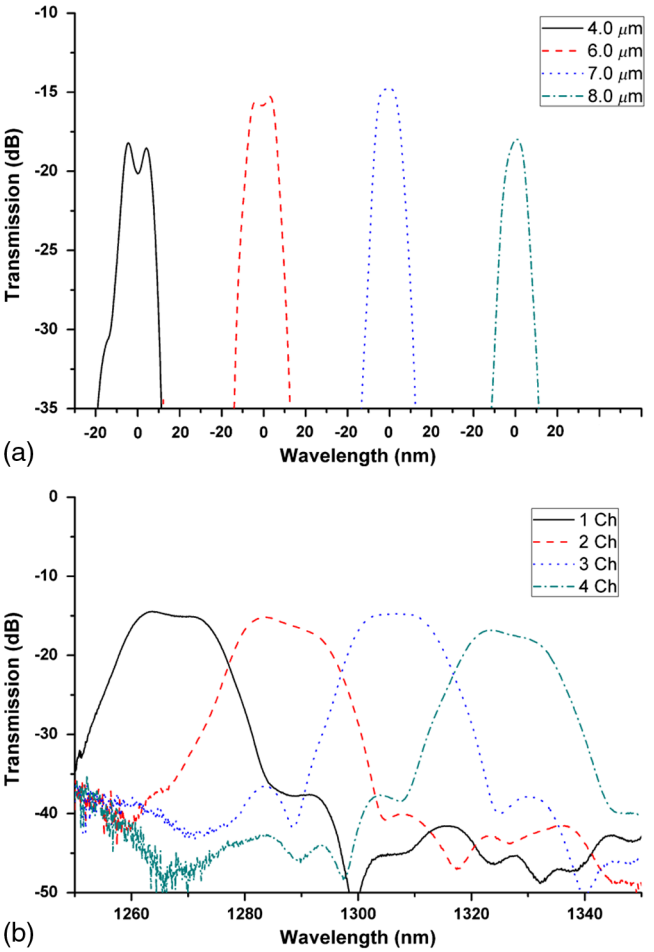

Fig. 9 Measurement spectral response of (a) MMI-PCG with variation of input taper width w and (b) MMI-PCG with 7.0 μm wide input taper.

−14.8 dB. There is about a −3 dB loss resulting from the flat top response. The remaining loss is believed to be mainly due to grating facet imperfections such as nonverticality, corner rounding, and sidewall roughness. The crosstalk of the present fabricated device is −22 dB, and the on-chip loss nonuniformity is 2.5 dB. Compared with the simulation results, there is about 10 nm of spectral shift in the transmission spectrum toward shorter wavelengths. This is believed to be caused by the thinner planar waveguide of the fabricated PCG and its slightly smaller effective RI of planar waveguide mode than the simulation. Thus, we have successfully achieved a flattened spectral response by adjusting the input taper width w of the MMI aperture structure.

6 Conclusion

In summary, we have demonstrated four-channel PCG wavelength demultiplexers with a flattened spectral response based on SU-8 polymer waveguides. The flattened spectral response to all spectrally separated channels is accomplished by using an optimized MMI as the input aperture to the PCG planar waveguide. The mode field distribution at the planar waveguide input aperture is controlled by adjusting the width w of the input taper connected to the MMI. The devices were realized on SU-8 polymer waveguides by one-step UV lithography. Experimental results confirm that the shape of spectral response can be controlled by adjusting the input taper width. The PCG-based wavelength demultiplexer with a flattened spectral response can be widely used for dense or coarse WDM systems to support various optical interconnection and communication applications.

Acknowledgments

This project was supported by the National Science Foundation under Grant No. ECCS 0901533. The authors would like to thank Sung Jin Kim, Young-hun Paik, and Hossein Shokri-Kojori for useful technical discussions.

References

1. K. Okamoto, "Wavelength-division-multiplexing devices in thin SOI: advances and prospects," *IEEE J. Sel. Top. Quantum Electron.* **20**(4), 8200410 (2014).
2. S. Janz et al., "Planar waveguide echelle grating in silica-on-silicon," *IEEE Photonics Technol. Lett.* **16**(2), 503–505 (2004).
3. S. Cheung et al., "Ultra-compact silicon photonics 512 × 512 25 GHz arrayed waveguide grating router," *IEEE J. Sel. Top. Quantum Electron.* **20**(4), 8202207 (2014).
4. N. Juhari et al., "Optimal design of linear tapered double S-shaped arrayed waveguide grating for broad channel spacing on silicon-on-insulator," *Opt. Eng.* **53**(8), 087110 (2014).
5. J. Brouckaert et al., "Planar concave grating demultiplexer fabricated on a nanophotonic silicon-on-insulator platform," *IEEE J. Lightwave Technol.* **25**(5), 1269–1275 (2007).
6. D. Feng et al., "Fabrication insensitive echelle grating in silicon-on-insulator platform," *IEEE Photon. Tech. Lett.* **23**(5), 284–286 (2011).
7. X. Chen et al., "Planar concave grating demultiplexer for coarse WDM based on confocal ellipses," *Opt. Commun.* **237**, 71–77 (2004).
8. D. Feng et al., "Compact single-chip VMUX/DEMUX on the silicon-on-insulator platform," *Opt. Express* **19**(7), 6125–6130 (2011).
9. S. Pathak et al., "Optimized silicon AWG with flattened spectral response using an MMI aperture," *IEEE J. Lightwave Technol.* **31**(1), 87–93 (2013).
10. G. Jiang et al., "Planar concave grating with flattened spectral response for wavelength demultiplexing optical interconnection," *Proc. SPIE* **9368**, 93680R (2015).
11. V. I. Tolstikhin et al., "Monolithically integrated optical channel monitor for DWDM transmission systems," *IEEE J. Lightwave Technol.* **22**(1), 146–153 (2004).
12. H. Li et al., "Practical fabrication and analysis of an optimized compact eight-channel silicon arrayed-waveguide grating," *Opt. Eng.* **52**(6), 064602 (2013).
13. G. Jiang et al., "Slab-modulated sidewall Bragg gratings in silicon-on-insulator ridge waveguides," *IEEE Photonics Technol. Lett.* **23**(1), 6–8 (2011).
14. K. S. Chiang, "Development of optical polymer waveguide devices," *Proc. SPIE* **7605**, 760507 (2010).
15. G. Jiang, S. Baig, and M. R. Wang, "Flexible polymer waveguides with integrated mirrors fabricated by soft lithography for optical interconnects," *J. Lightwave Technol.* **31**(11), 1835–1841 (2013).
16. D. Dai et al., "Compact microring resonator with 2 × 2tapered multimode interference couplers," *IEEE J. Lightwave Technol.* **27**(21), 4878–4883 (2009).
17. B. Yang et al., "Fabrication and characterization of small optical ridge waveguides based on SU-8 polymer," *IEEE J. Lightwave Technol.* **27**(18), 4091–4096 (2009).
18. M. Nordström et al., "Single-mode waveguides with SU-8 polymer core and cladding for MOEMS applications," *IEEE J. Lightwave Technol.* **25**, 1284–1289 (2007).
19. K. K. Tung, W. H. Wong, and E. Y. B. Pun, "Polymeric optical waveguides using direct ultraviolet photolithography process," *Appl. Phys. A* **80**(3), 621–626 (2005).
20. C. Y. Chao, W. Fung, and L. J. Guo, "Polymer microring resonators for biochemical sensing applications," *IEEE J. Sel. Top. Quantum Electron.* **12**(1), 134–142 (2006).
21. .M. C. Hutley, "Concave gratings," in *Diffraction Grating*, Academic, New York, pp. 215–262 (1982).
22. L. B. Soldano and E. C. M. Pennings, "Optical multi-mode interference devices based on self-imaging: principles and applications," *IEEE J. Lightwave Technol.* **13**(4), 615–629 (1995).
23. R. J. Lycett, D. F. G. Gallagher, and V. J. Brulis, "Perfect chirped echelle grating wavelength multiplexor: design and optimization," *IEEE Photonics J.* **5**(2) 2400123 (2013).

Guomin Jiang received his BS degree in applied physics from the University of Electronic Science and Technology of China, Chengdu, China, in 2008 and received his MS degree in microelectronics and solid state electronics from Zhejiang University, Hangzhou, China, in

2011. He received his PhD in electrical and computer engineering from the University of Miami, Coral Gables, Florida, in 2015. His research interests include integrated optics, optical interconnects, optical communication, and microfluidic systems.

Sarfaraz Baig received his BSEE degree in 2006 and MSECE degree in 2008 from the University of Miami, Coral Gables, Florida. Currently, he is pursuing his PhD in biomedical engineering at the University of Miami. His research interests include optical imaging, holography, integrated photonics, and optical interconnects.

Hui Lu received her BS degree in electrical engineering from Tianjin University, Tianjin, China, in 2007. She received her MS degree in optics from Shanghai Institute of Optics and Fine Mechanics, Chinese Academy of Sciences, Shanghai, China, in 2010. Currently, she is pursuing her PhD in electrical and computer engineering at the University of Miami, Coral Gables, Florida. Her research interests are reflectometry and optical coherence tomography for noninvasive high-resolution eye imaging.

Kai Shen received his BS degree in physics in 2008 and his MS degree in microelectronics and solid state electronics in 2010 from Wuhan University, Wuhan, China. Currently, he is pursuing his PhD in electrical and computer engineering at the University of Miami. His research interests include photonic crystals, quantum dots-based light sources, and super-resolution imaging.

Michael R. Wang received his PhD in electrical and computer engineering from the University of California, Irvine, in 1992. Currently, he is a full professor of electrical and computer engineering at the University of Miami. He has been a principal investigator and/or project manager of more than 50 U.S. government–sponsored research projects. He has authored and coauthored more than 190 journal papers, proceedings, and conference presentations. He is a fellow of SPIE.